Influence of AWGN on the Possibility to Remove a Continuous Wave EM Disturbance in OFDM systems

Aleksandr Ovechkin
ESAT-WaveCore, M-Group
KU Leuven, Bruges Campus
B-8200 Brugge, Belgium
aleksandr.ovechkin@kuleuven.be

Brian Leeman
ESAT-WaveCore, M-Group
KU Leuven, Bruges Campus
B-8200 Brugge, Belgium
brian.leeman@kuleuven.be

Dries Vanoost
ESAT-WaveCore, M-Group
KU Leuven, Bruges Campus
B-8200 Brugge, Belgium
dries.vanoost@kuleuven.be

Tim Claeys
ESAT-WaveCore, M-Group
KU Leuven, Bruges Campus
B-8200 Brugge, Belgium
tim.claeys@kuleuven.be

Guy A. E. Vandenbosch
ESAT-WaveCore
KU Leuven
3001 Leuven, Belgium
guy.vandenbosch@kuleuven.be

Davy Pissoort
ESAT-WaveCore, M-Group
KU Leuven, Bruges Campus
B-8200 Brugge, Belgium
davy.pissoort@kuleuven.be

Abstract—In the era of wireless technologies, orthogonal frequency division multiplexing (OFDM) techniques and their modifications gained huge popularity. Despite all their benefits they still have several Achilles' heels. One of them is the negative influence of a narrowband or continuous wave (CW) electromagnetic disturbance (EMD). In this paper, a specific CW EMD removal algorithm for OFDM communication systems was investigated for its stability when both a CW EMD and additive white Gaussian noise (AWGN) were affecting the OFDM communication system. By using the spectral leakage phenomenon, the algorithm estimates a mismatch between the subcarriers and CW EMD frequencies and subsequently calculates all the needed CW parameters, i.e. amplitude and phase. The goal of the investigation was to find out which modulation scheme gives the best algorithm's performance. Therefore after a number of simulations on the algorithm with different power variations of CW EMD and AWGN, the results turned out to be better when lower order modulation schemes were in use. These results were explained in the frequency domain as the AWGN's fraction with regard to the CW EMD error was minimum within the subcarriers close to the CW EMD's frequency bin and much higher for other subcarriers. In the end, prepositions on how to maximise the CW removal algorithm's performance under simultaneous CW EMD and AWGN were outlined.

Index Terms—Orthogonal frequency division multiplexing (OFDM), continuous wave noise, electromagnetic disturbance (EMD), narrowband interference (NBI), noise cancellation, additive white Gaussian noise (AWGN)

I. INTRODUCTION

Wireless communication technologies are ubiquitous in our daily life. For example, in the year 2000, there were only 740 million mobile subscriptions, now this number is more than 8.6 billion [1]. For different purposes one may find numerous wireless technologies with various modulation techniques: Bluetooth with, first, Gaussian frequency-shift keying and later differential quadrature phase-shift keying, Zigbee with binary phase-shift keying and offset quadrature phase-shift keying modulation for different frequencies. There is also a series of IEEE 802.11 standards that started with direct sequence and frequency hopping spread spectrum modulation techniques for their early versions (IEEE 802.11-1997, IEEE 802.11 b) and later switched to orthogonal frequency division multiplexing (OFDM) techniques and their modifications. OFDM is not solely used in IEEE 802.11 standards series, it is also present in audio and video broadcasting, and in 4G [2] and 5G [3].

OFDM gained its popularity due to specific advantages. First, it is bandwidth-efficient since it divides its bandwidth into multiple overlapping subcarriers orthogonal to each other. This means that power spectral density of one subcarrier reaches its maximum while others have zero power. As a consequence, the intercarrier interference is minimised. Next, the intersymbol interference from the previous OFDM symbol can be eliminated by using the cyclic prefix. It also helps with channel estimation and equalisation and is especially useful in a multipath fading environment [4]. With all the OFDM's advantages, there are a number of disadvantages, for example, a high dependency on frequency synchronisation, sensitivity to Doppler fading and high peak-to-average power ratios. OFDM is also prone to continuous wave (CW) electromagnetic disturbances (EMDs) [5].

CW EMDs become a bigger threat for OFDM systems when a spectral leakage phenomenon occurs. Without the CW EMD, the signal is phase locked at the receiver's side and coherently sampled. Nevertheless, with the addition of CW EMD, the received signal is mixed with the disturbance that most likely

does not coincide by phase and frequency with the transmitted signal. Therefore non-coherent sampling occurs resulting in power leakage to multiple subcarriers, i.e. spectral leakage. In this case, the subcarriers close to the actual CW EMD frequency are affected the most [6]. This can result in bit flips and incorrect signal demodulation which is intolerable in safety-critical applications like autonomous driving or industry 4.0 applications where the OFDM technique is used. For example, the 5G system for Factories of the Future should be able to provide 1 ms latency for precise cooperative robotic motion control. The message size should be between 40 and 250 bytes [7]. This means that the system will be unlikely to retransmit the message, hence it should arrive from the first go. Therefore OFDM systems should be robust and resilient in harsh electromagnetic (EM) environments.

CW EMD or a narrowband EMD has recently been tackled by different research groups. A novel CW EMD removal algorithm for OFDM systems was proposed [6]. The mathematical model that is used as a basis for that algorithm works in the following fashion. First, it estimates a difference between the main carrier and the CW EMD frequency. Based on this frequency difference, the CW EMD parameters: amplitude and phase are calculated. Knowing all the disturbance parameters the CW EMD can be reconstructed and subsequently subtracted from the signal.

This paper sheds some light on the work of the algorithm with the presence of the additive white Gaussian noise (AWGN). In the paper, the algorithm's performance is tested by making a number of simulations with different AWGN and CW EMD parameters. Based on the simulation results and conducted analysis the modulation schemes' choice recommendations leading to the best algorithm's performance are formulated.

Therefore the remainder of the paper is organised as follows: Section II provides the algorithm's basics that are crucial for understanding the follow-up analysis. Section III shows the simulation framework depicting all the variables and their values. Section IV discusses the algorithm's performance for different AWGN and CW EMD power levels. The simulation results are shown in heatmaps for different modulation order schemes. Section V further explains the simulation results providing an analysis of different modulation scheme orders constellation and spectrum diagrams explaining the algorithm's response to AWGN. Section VI draws concluding remarks.

II. BASICS OF THE CW REMOVAL ALGORITHM

To assist the reader in the understanding of the CW EMD removal algorithm, we provide here a summary of Section II of [6]. The algorithm starts by predicting the error mismatch E_m^* (m is a subcarrier number) between the received signal and the demodulated symbols. When E_m^* exceeds the quarter minimum Euclidean distance between contiguous symbols on the QAM constellation, the removal algorithm removes a possible CW EMD. To go a bit more in-depth, E_m^* is obtained by subtracting the received symbols, R_m, after DFT from the demodulated and re-modulated S_m^* symbols. Here, index m denotes a subcarrier number and * indicates the potentially erroneously obtained symbols due to the re-modulation process shown in Fig. 1. For example, if the error is low, a symbol flip does not occur and a S_m^* symbol is remapped back to the received one R_m. This will result in E_m either close or equal to zero. Nevertheless, if the CW EMD could cause a symbol flip, then the remapped S_m^* symbol will not coincide with R_m and result in the error E_m^*.

The essence of the algorithm along with the re-modulation and obtaining E_m^* values are shown in Fig. 1. When a single E_m^* value is greater than the quartered minimum Euclidean distance between adjacent I—Q points, the algorithm can be split into the following steps:

1. The frequency difference f_{diff} between the carrier and CW EMD frequencies is calculated for $m \in [0:K/2]$ using the following expression:

$$f_{\text{diff}} = \frac{jBd}{2\pi} ln \left(\frac{E_m - E_{m+\frac{K}{2}}}{E_m + E_{m+\frac{K}{2}}} e^{j2\pi m/K} \right), \quad (1)$$

where Bd is the baud rate, K is the number of subcarriers which is an even number.

2. The resulted set of f_{diff} values is swept through to find the most probable one:

   a) The five f_{diff} values that have closest to zero imaginary $Im(f_{\text{diff}})$ values are taken.

   b) The estimated f_{diff} value is obtained by taking the median of $Re(f_{\text{diff}})$ from the five values obtained in the previous step.

3. The CW EMD phase θ_{CW} and amplitude A_{CW} estimations are calculated by:

$$A_{\text{CW}} = \left| \frac{E_m + E_{m+\frac{K}{2}}}{\sum\limits_{n=0}^{K-1} \left(e^{-j2\pi n(f_{\text{diff}}/Bd + m/K)} \left(1 - e^{-j\pi n} \right) \right)} \right|, \quad (2)$$

where n represents a subcarrier number.

$$\theta_{\text{CW}} = j \ln \left(\frac{(A_{\text{CW}})^{-1}(E_m + E_{m+\frac{K}{2}})}{\sum\limits_{n=0}^{K-1} \left(e^{-j2\pi n(f_{\text{diff}}/Bd + m/K)} \left(1 - e^{-j\pi n} \right) \right)} \right).$$
$$(3)$$
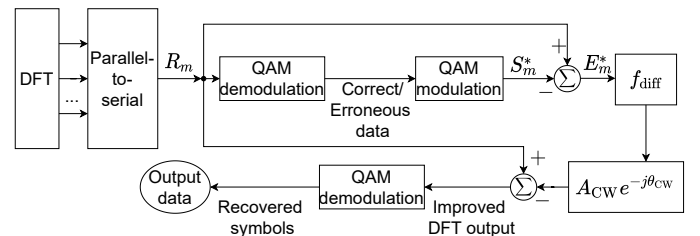
Fig. 1. The CW EMD excision procedure in OFDM at the receiver's side [6]

4. When all the CW EMD parameters are known, the CW EMD error is calculated:

$$E_m = A_{CW} \sum_{n=0}^{K-1} \left(e^{-j(2\pi f_{diff} n / Bd + \theta_{CW})} e^{-j2\pi mn/K} \right). \quad (4)$$

5. The CW EMD error E_m is subtracted from the received R_m symbols resulting in the improved DFT symbols.

The further demodulation of the improved DFT symbols will result in recovered symbols. An in-depth mathematical derivation of the algorithm can be found in [6].

III. SIMULATION FRAMEWORK

Simulations were performed with a few assumptions. First, the OFDM system was fully synchronized in both the time and frequency domains. Second, perfect multipath fading equalization was assumed in order not to complicate the system with pilot symbols and cyclic prefixes, so they were not used. Simulations took place in baseband frequencies.

Simulation parameters can be split into two tables: for OFDM symbols (Table I) and CW EMD with AWGN (Table II). Since these tests aim to define the best communication parameters' settings for the highest algorithm's performance, the bits number, Y, was preserved to be constant throughout simulations. AWGN was defined by a Signal-to-noise ratio (SNR). Signal-to-interference ratio (SIR) for CW EMD was defined as follows:

$$SIR = 20 \log_{10} \left(\frac{A_s}{A_{CW}} \right), \quad (5)$$

where A_s and A_{CW} denote the amplitude of the signal and interference, respectively.

The parameter α defines the position of CW EMD with regards to the subcarriers in such a way that α equal to 0 or 1 means that the CW EMD coincides with a subcarrier. α was set to 0.5 to have the highest spectral leakage impact on the received signal R_m.

Since a CW EMD is a narrowband electromagnetic disturbance, one may assume it as a burst error. Interleaving techniques proved to be effective against these types of disturbances [8]. Therefore to further improve the performance of the algorithm the Hamming(15,11) coding and a row-column interleaving were implemented. The simulation results presented in Figs. 2a — 2d are averaged over 360 CW EMD phases per each SIR and SNR value.

IV. SIMULATION RESULTS

The performance of the CW EMD removal algorithm in OFDM for different QAM constellations is presented on heatmaps in Figs. 2a — 2c. The performance is evaluated using the bit error rate (BER) parameter. For reference, the QPSK performance without the algorithm but with the Hamming coding is shown in Fig. 2d.

Using a colour palette in Figs. 2a — 2d, the BER intensity is shown. The darker colours represent low BER values while for the brighter colours it is vice versa. Looking at Fig. 2a, one may notice that the SNR level of -15 dB makes the

Parameter	Value
Modulation scheme[a]	QAM(M), M= [4; 16; 64]
Number of subcarriers, K, divided by subcarrier width	[240; 120; 80]
Number of bits, Y	480
Baud rate, Bd	100
Coding technique	Hamming code(15,11)+interleaving
Subcarrier width, H	Bd/K

[a] When the modulation order M is set to 4, then the modulation scheme is QPSK.

algorithm completely unable to distinguish the CW EMD and results in a BER of ≈ 45 % throughout the whole SIR span. Talking about the SIR span, it stretches from -30 dB to 50 dB (see Table II). For example, in [9] the noise levels for different frequency bands were much higher. In particular, for an interferer working in the instrumental, scientific and medical (ISM) band of 2.4 GHz, the measured mean CW EMD power reached around -60 dBm. However, it was not the purpose of our simulations to test the algorithm's performance for a broad SIR span since it has already been done in [6]. Going back to Fig. 2a and analysing the simulation results for higher, more probable SNR and SIR levels, one may notice that for the SNR value of 15 dB, the BER value does not exceed 11.1 %. For SNR levels of 25 and 35 dB, the algorithm can achieve errorless performance starting from SIR ≥ 40 dB and SIR ≥ 30 dB, respectively.

If we compare the results in Fig. 2a with the ones in Fig. 2d, one may find that the Hamming coding helps especially when

Parameter	Value
CW EMD phase[a](θ_{CW}), degree	[0:359]
Distance to the closest to CW EMD subcarrier,[b] α	0.5
SIR span, dB	[-30:50]
SIR step, dB	10 dB
SNR span, dB	[-15:35]
SNR step, dB	10 dB
CW EMD amplitude,[c] A_{CW}	$A_{CW} = \frac{S_{RMS}}{10^{SIR/20}}$

[a] Per each phase θ_{CW}, a new sequence of bits Y was generated;

[b] f_{CW} and f_c are aligned in such a way that f_{diff} can take values between -50 Hz and 50 Hz;

[c] S_{RMS} is the root-mean-squared value of the signal in the time domain.

the SNR and SIR levels are high, therefore the performance with the sole Hamming coding (Fig. 2d) outperforms the algorithm's performance case (Fig. 2a). Nevertheless, this improvement is negligible and fades away starting when the SIR ≤ 0 dB. For example, throughout the whole SIR span at an SNR level of 25 dB, the algorithm has the highest BER at SIR equal to -30 dB which is around 2.2 %, while for the reference case the BER varies from 0 % to around 44 %.

The BER results differ for the higher modulation order schemes whose results are presented in Figs. 2b and 2c. For example, in Fig. 2b the lowest BER value for the highest SNR that is equal to 35 dB is 28.7 %. For QAM64, presented in Fig. 2c, this value is even higher and reaches 39.5 %. Both Figs. 2b and 2c contain errorless results, although they are limited to SIR levels happening at an SNR equal 35 dB and starting from SIR ≥ 40 dB and SIR ≥ 50 dB, respectively. If one assumes that a packet loss of 1 % of data is considered to be acceptable, then with QPSK the OFDM system can potentially perform well, according to results, when SIR ≥ -30 dB and SIR ≥ -20 dB for an SNR equal to 35 and 25 dB, respectively. For QAM16 the working range decreases to SIR ≥ 20 dB and SIR ≥ -10 dB for an SNR equal to 35 and 25 dB, respectively. For QAM64, this range shrinks even more, the algorithm has a BER ≤ 1 % only for an SNR equal to 35 dB with an SIR ≥ 30 dB. If one implements a rule-of-a-thumb for telecommunications applications with an allowed BER equal to 10^{-9}, the working range of the algorithm will be even more limited. The reference cases for Figs. 2b and 2c are very similar and correlate with Fig. 2d and are therefore not shown.

Heatmaps presented in Figs. 2b — 2c clearly show the better performance for lower orders modulation schemes. However, in order to explain this, a more detailed look at the frequency spectrum of the received signal has to be made.

V. THE ALGORITHM'S QAM CONSTELLATION AND SPECTRUM ANALYSIS

For a better understanding of why CW EMD performs better with lower QAM schemes, let us look at QAM constellation diagrams. Fig. 3 depicts a QPSK constellation diagram. To not overload the figure with data, only four subcarriers are shown. The diagram presents the reference signal (blue stars) and disturbed received signals with both CW & AWGN (red squares) and only with CW (green triangles). The error between the reference symbol and the received one is outlined with a vector $\vec{E}$. It can be seen that the total error vector is composed of CW and AWGN vectors, so $\vec{E}^{\text{Total}} = \vec{E}^{\text{CW}} + \vec{E}^{\text{AWGN}}$. It can be noticed that $\vec{E}_1^{\text{AWGN}}$, $\vec{E}_2^{\text{AWGN}}$, $\vec{E}_3^{\text{AWGN}}$ do not influence the demodulation process of the received symbols. Symbol 2 is disturbed and causes a symbol flip. However, AWGN for this received symbol ($\vec{E}_2^{\text{AWGN}}$) does not affect the demodulation process. For the first and third symbols, there is no symbol flip and AWGNs $\vec{E}_1^{\text{AWGN}}$, $\vec{E}_3^{\text{AWGN}}$ do not affect the demodulation outcome. A completely different story happens with the fourth symbol where AWGN $\vec{E}_4^{\text{AWGN}}$ is high enough to displace the
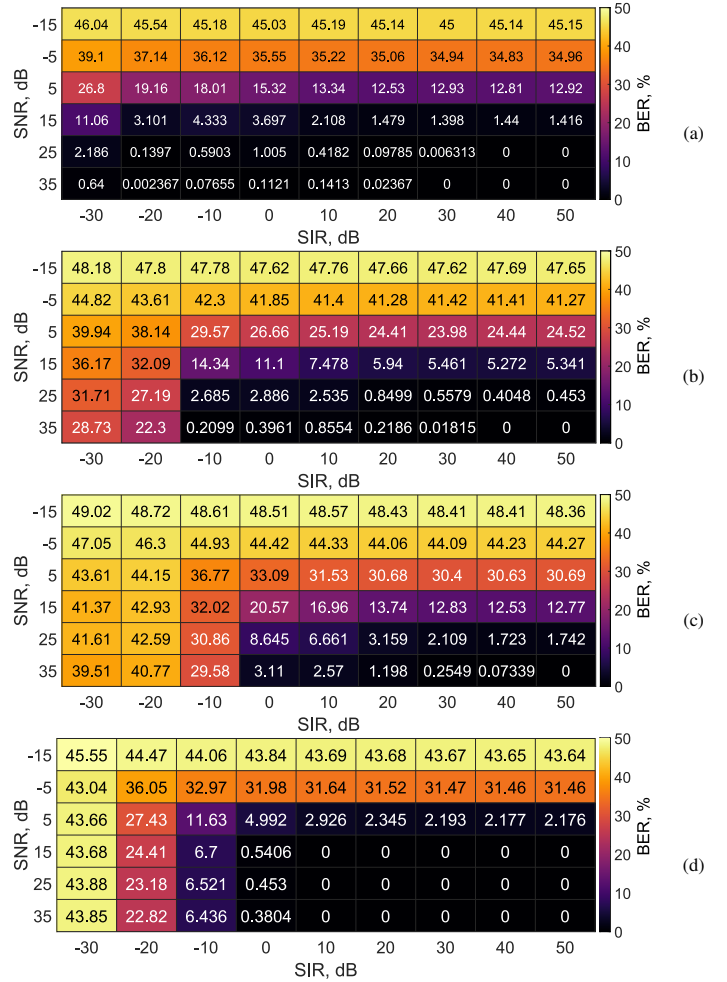
Fig. 2. The BER performance of the CW removal algorithm under the influence of AWGN and CW EMD for different modulation order schemes with various subcarrier numbers: (a) QPSK with 240 subcarriers, (b) QAM16 with 120 subcarriers, (c) QAM64 with 80 subcarriers, (d) the reference case without the algorithm but with the Hamming coding.

symbol to the other quadrant resulting in a symbol flip, wrong demodulation and potentially wrong CW EMD estimation by the algorithm. Now let us look at the higher constellation order modulation. Fig. 4 represents a QAM64 constellation diagram. The simulation parameters for its generation are the same as for Fig. 3, however, the number of subcarriers is different and set to 64. For the figure readability, received symbols disturbed by both CW EMD and AWGN (red squares) and by only CW (green triangles) are presented for only 16 subcarriers. The reference QAM64 symbols are shown with blue circles for all the 64 subcarriers. The area in which a symbol can be correctly demodulated is outlined by the black dashed circles. It can be seen that, for example, for area 1 the received symbols both disturbed by CW EMD and AWGN and by CW EMD are in the area. The same cannot be noticed for area 2 where the received symbol disturbed by CW EMD is still inside the circle while the same symbol disturbed by CW EMD and AWGN is outside the circle. A similar explanation is applicable for
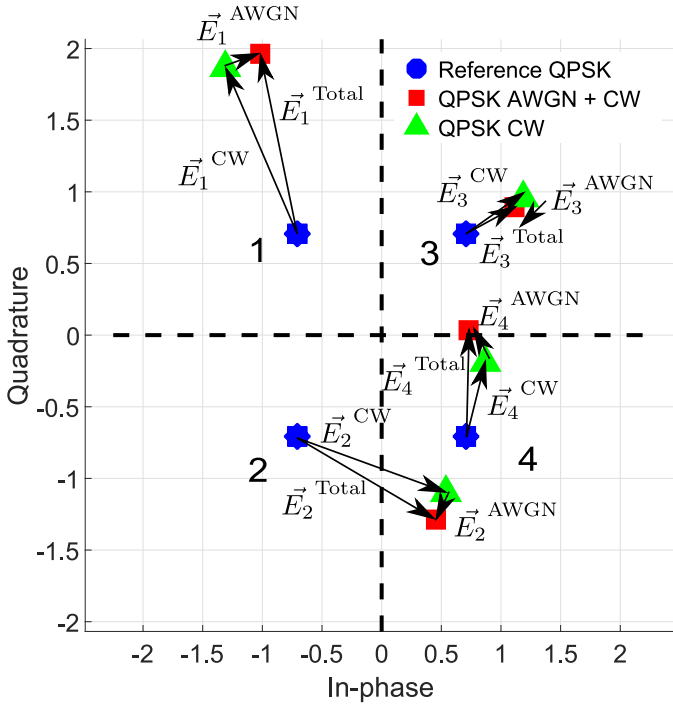
Fig. 3. A QPSK constellation diagram with 4 subcarriers with SIR = 0 dB, SNR = 15 dB, $\Theta_{CW} = 50°$

the remaining symbols. It can be seen that for the higher modulation scheme order the correct demodulation area is smaller resulting in more symbol flips due to the AWGN. This completely breaks the pattern of the CW EMD in the received signal making the CW EMD almost impossible to estimate correctly using the algorithm. To further analyse the influence of the AWGN's error component $\vec{E}^{AWGN}$ in the total error $\vec{E}^{Total}$ let us look at frequency diagrams of the spectrum (Figs. 5a and 5c). These figures show the absolute induced error of the received signal disturbed by CW EMD and AWGN per subcarrier in the frequency domain. From Figs. 5a and 5c one may calculate the AWGN's relation towards the CW EMD and its influence on the total error. For this, a few mathematical equations have to be shown.

To get the AWGN's component, one may need, first, to get the total error E_m^{Total}. It can be calculated by subtracting the data in the frequency domain at the transmitter's side S_m before transmission from the received data right after the DFT block at the receiver's side R_m.

With the total error E_m^{Total} at hand, the AWGN component E_m^{AWGN} can be found by subtracting from the total error E_m^{Total} the generated CW EMD component E_m^{CW}. Prior to that, let us transform the generated CW EMD component in the time domain $E_n^{CW}(t)$ to the frequency domain by performing a DFT.

$$E_m^{CW} = \sum_{n=0}^{K-1} E_n^{CW}(t)e^{-j2\pi mn/K}, \qquad (6)$$

where n is the sample number and coincides with the subcarrier number defined earlier in (2) — (4).

Then the AWGN component E_m^{AWGN} will be obtained as:

$$E_m^{AWGN} = E_m^{Total} - E_m^{CW}. \qquad (7)$$

With all the needed parameters in the frequency domain, the AWGN's error fraction in the CW EMD error will be:

$$\delta_m^{AWGN} = \frac{|E_m^{AWGN}|}{|E_m^{CW}|} \cdot 100\%. \qquad (8)$$

$$E_m^{Total} = R_m - S_m. \qquad (9)$$

Equation (8) was used for making Figs. 5b and 5d. Comparing Figs. 5a, 5c with 5b and 5d one may notice a tendency: the higher the presence of CW EMD in the received signal (subcarriers 119, 120 and 39, 40 for Figs. 5a and 5c, respectively), the lower the AWGN's component towards the CW EMD error component. Hence the AWGN's component in the total error is also lower. Due to spectral leakage, only the subcarriers close to the CW EMD's frequency are influenced the most resulting in the higher CW EMD's error values whereas the influence of AWGN on subcarriers is equal on average. Therefore δ_m^{AWGN} is higher on the sides and gradually decreases to minimal values in the region of subcarriers 118 — 123 and 39 — 41 in Figs. 5b and 5d, respectively. The CW EMD removal algorithm presented in [6] relies on all the subcarriers and tolerates worse high error fluctuations due to AWGN in the regions where the CW EMD component is relatively low. Therefore it is preferable to use the algorithm with lower order modulation schemes to have a bigger distance between symbols which will decrease the probability of symbol flip and ease the error estimation and the subsequent demodulation process.
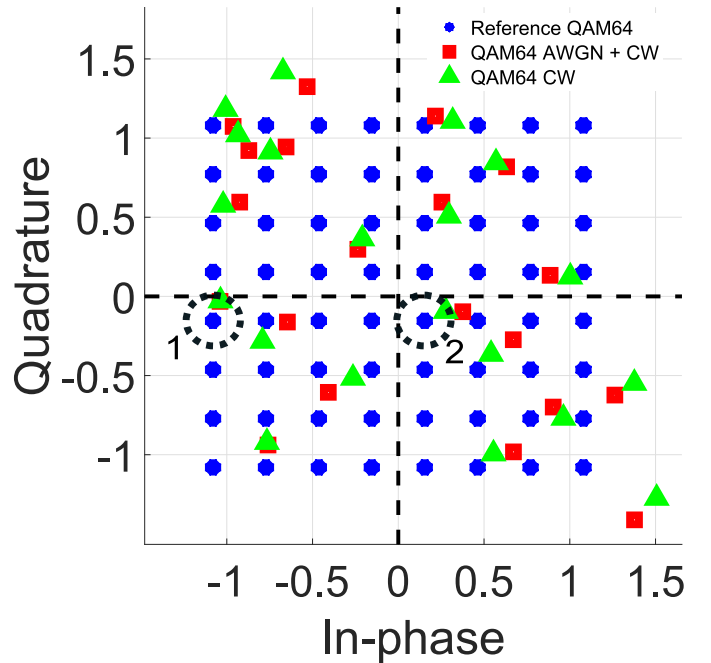
Fig. 4. A magnified QAM64 constellation diagram with 64 subcarriers with SIR = 0 dB, SNR = 15 dB, $\Theta_{CW} = 50°$
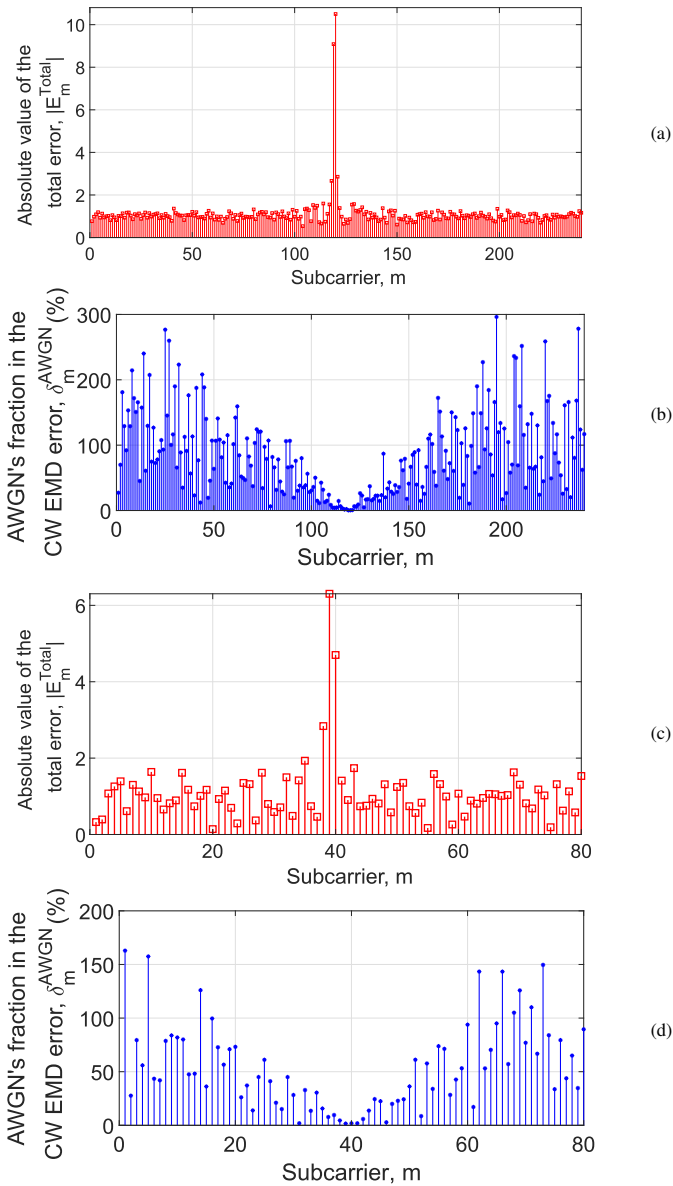
Fig. 5. Frequency spectrum diagrams for QPSK with 240 subcarriers (a, b) and QAM64 with 80 subcarriers (c, d) with SIR = 0 dB, SNR = 15 dB, $\Theta_{\mathrm{CW}} = 50°$: (a) The absolute received signal disturbed by both CW and AWGN, (b) An AWGN's error fraction $\vec{E}_m^{\mathrm{AWGN}}$ towards the CW EMD error E_m^{CW} in %, (c) The absolute received signal disturbed by both CW and AWGN, (d) An AWGN's error fraction $\vec{E}_m^{\mathrm{AWGN}}$ towards the CW EMD error $E_m^{\vec{\mathrm{CW}}}$ in %.

VI. CONCLUSION

This paper shows how to optimally use the algorithm proposed in [6] in a harsh electromagnetic environment consisting of both a CW EMD and AWGN. In [6], it has been demonstrated that for a disturbance frequency not equal to one of the OFDM subcarriers, the algorithm can estimate the disturbance frequency with high precision, resulting in a gain of more than 80 dB when compared to the case without the algorithm. The proposed optimization strategy for the same payload decreases the BER by approximately 41 % for an SIR of -30 dB and SNR of 25 dB. This results in a drastic increase in OFDM communication availability and dependability especially for safety-critical systems.

The paper contains the results of multiple simulations with different SNR and SIR levels but with a constant number of bits. The results showed a drastic difference in the BER response between different order modulation schemes. For example, for QPSK with 240 subcarriers and QAM64 with 80 subcarriers for an SIR of -30 dB and SNR of 25 dB one may get 2.2 % and 41.6 % BER, respectively. In-phase and quadrature constellations along with frequency diagrams show that higher modulation order schemes are more congested and therefore are more prone to a symbol flip. Finally, the AWGN's component fraction in the CW EMD error per subcarrier in the frequency domain was calculated. Taking into account the fact that the algorithm presented in [6] relies on the values of all the subcarriers, the error values fluctuation caused by the AWGN's component can be detrimental. Therefore for the best CW EMD removal algorithm's performance, one may consider the lowest possible modulation order scheme.

The topic of CW EMD in OFDM signals is relevant, especially in safety-critical systems. Therefore further research directions will focus on the algorithm's validation, first in the lab scenario and then in the real environment. The other research topic, which is currently in process, will be centred around reducing the algorithm's dependency on AWGN's fluctuations.

REFERENCES

[1] "Mobile Communications - Statistics & Facts," statista.com. https://www.statista.com/topics/1147/mobile-communications/#dossierKeyfigures/, (accessed: February 17, 2022), year=2022.

[2] "3rd Generation Partnership Project; Technical Specification Group Radio Access Network; Evolved Universal Terrestrial Radio Access (E-UTRA); Physical channels and modulation (Release 17)," 3rd Generation Partnership Project, Valbonne , France, Standard, Dec. 2021.

[3] "3rd Generation Partnership Project; Technical Specification Group Radio Access Network; NR; Physical channels and modulation (Release 17)," 3rd Generation Partnership Project, Valbonne , France, Standard, Dec. 2021.

[4] A. Goldsmith, *Multicarrier Modulation*. Cambridge University Press, 2005, p. 374–402.

[5] A. Ovechkin, T. Claeys, D. Vanoost, J. F. Dawson, G. A. E. Vandenbosch, and D. Pissoort, "Characterizing the robustness of wi-fi and bluetooth against continuous wave em disturbances inside a reverberation chamber," in *2021 IEEE International Joint EMC/SI/PI and EMC Europe Symposium*, 2021, pp. 1031–1036.

[6] A. Ovechkin, T. Claeys, D. Vanoost, G. A. E. Vandenbosch, and D. Pissoort, "A novel method of removing the influence of continuous electromagnetic wave disturbances in ofdm systems," *IEEE Transactions on Electromagnetic Compatibility*, pp. 1–10, 2021.

[7] "3rd Generation Partnership Project; Technical Specification Group Services and System Aspects; Study on Communication for Automation in Vertical Domains (Release 16) ," 3rd Generation Partnership Project, Valbonne , France, Standard, Dec. 2021.

[8] Y. Shi, X. M. Zhang, Z.-C. Ni, and N. Ansari, "Interleaving for combating bursts of errors," *IEEE Circuits and Systems Magazine*, vol. 4, no. 1, pp. 29–42, 2004.

[9] A. Palaios, V. M. Miteva, and P. Mähönen, "Contemporary study of radio noise characteristics in diverse environments," *IEEE Access*, vol. 6, pp. 25 621–25 631, 2018.